Clinopyroxene/Melt Partitioning: Models for Higher Upper Mantle Pressures Applied to Sodium and Potassium

Julia Marleen Schmidt
Institute of Geological Sciences)
Freie Universität Berlin
Berlin, Germany
email: julia.schmidt@fu-berlin.de

Lena Noack
Institute of Geological Sciences
Freie Universität Berlin
Berlin, Germany
email: lena.noack@fu-berlin.de

***Abstract*—Mineral/melt partition coefficients describe the redistribution of trace elements during melting processes. They are highly influenced by changing pressure, temperature, and composition. We find that for sodium, partition coefficients rise in the order of two magnitudes from 0-15 GPa along the peridotite solidus temperature. Still, because of lacking high-pressure experimental data and the limited pressure range of most partitioning models, mantle and crust evolution models normally rely on constant partition coefficients. This is especially unfavorable for models which want to explore the thermal evolution of a terrestrial planet by tracing the heat producing elements. Based on a thermodynamic model, we parametrise sodium partitioning equations which are applicable from 0-12 GPa and 1410-2350 K. With the help of the sodium partitioning model, we calculate clinopyroxene/melt partition coefficients for the heat producing element potassium. Knowing both, the sodium and potassium partitioning behaviour, will help us to improve elemental redistribution calculations and therefore also thermal evolution models.**

Keywords*— *high-pressure partition coefficients; partial melting; thermodynamic modelling; trace element redistribution; radiogenic heat sources

I. Introduction

Inside the Earth and other terrestrial planets, partial melts usually control the redistribution of trace elements from the mantle to the crust. If melt is buoyant due to a lower density than the surrounding rock, it moves upwards and transports the previously incorporated incompatible trace elements towards the surface. This leads to enriched reservoirs near the surface and depleted upper mantle areas. Using thermodynamic models, the incorporation of an incompatible element can be predicted as has been outlined in [1] based on sodium as a reference for other trace elements. Expanding the redistribution concept to a larger number of elements (as is shown here exemplarily for the 1+ charge element potassium) leads to the creation of trace element patterns, which are unique geochemical markers of the events that led to the exact appearance and compositions of a rock of interest [2][3][4].

During melting, partition coefficients describe if an element prefers to be incorporated into a mineral or, if it is incompatible, into melt. Partitioning data for peridotite including the minerals olivine, orthopyroxene, and clinopyroxene show that in mantle rocks, clinopyroxene is the mineral taking in most incompatible trace elements [5][6]. This makes clinopyroxene the mineral with the largest influence on trace element redistribution.

Since partition coefficients of sodium between clinopyroxene and silicate melt are highly affected by changing pressure and temperature, partition coefficient models should consider these parameters. Because of analytical limitations, there are only few measured partition coefficients available for high-pressure conditions. Additionally, partition coefficient models are often only applicable for rather low pressures. This is the reason why so far, partial melt simulations in some mantle evolution models either neglected partition coefficients and chose pre-defined elemental abundances in mantle melts [7], or settled for constant experimentally derived and estimated partition coefficients [8][9][10][11].

In 1937, Goldschmidt postulated that both the matching size and charge of the mineral's lattice site and element of interest determine an element's ability to partition into a mineral [12]. This leads to the assumption that not only it is possible to determine the P-T sensitive partition coefficients experimentally, but also by means of numerical modelling. Based on a model of Brice (1975) [13], Blundy et al. (1995) [14] developed a quantitative model and determined a parametrised fit function for clinopyroxene/melt partition coefficients for sodium in the range of 0-4 GPa and 1000-1800°C. In Schmidt and Noack (2021) [1], this temperature and pressure range was already extended to higher pressure conditions, leading to a general parametrisation over a broad temperature range and pressures from 4-12 GPa. Here, we derive new parametrisations from surface to upper mantle conditions focusing on specific melt partitioning scenarios related to both formation and freezing of melt.

As is shown in Figure 1, partition coefficients of trace elements have a parabolic relationship in an Onuma diagram. The parabolas' curves change in broadness and shift along the x-axis depending on the bulk modulus E and the ideal lattice site radius r_0, respectively. Because of this relationship, it is

possible to calculate other trace elements' partition coefficients based on the reference coefficient D_{Na}.

The aim of this study is to implement a thermodynamic model for $D_{Na}^{cpx/melt}$ for a large range of pressures suitable for mantle melt simulations. Furthermore, we parametrise a scaling law from the mentioned model that is applicable for upper mantle pressures. This will open the possibility to include partition coefficients depending on pressure and temperature into mantle evolution models and to acquire more realistic model results [15].

After proving that both the thermodynamic models and the scaling laws are applicable, we derive clinopyroxene/melt partition coefficients for potassium from them. As one of the most abundant radiogenic elements, potassium is one of the largest contributors of heat inside the Earth [16][17]. Being able to calculate pressure and temperature dependent partition coefficients of potassium in clinopyroxene/melt provides us therefore an opportunity to make thermal evolution and mantle melting models more realistic.

The rest of the paper is organized as follows. In section II, we describe the methods used for our parametrisation, the thermodynamic model, and potassium partitioning in the appropriate subsections. Section III is dedicated to the results for the thermodynamic model, the parametrisations, and the application to potassium partitioning respectively. Section IV discusses the results and compares them to experimental data. Section V concludes the paper, summarizes the findings, and points out what can be done in future works.

II. Methods

A. Thermodynamic Model

To obtain the most realistic trace element partitioning results for mantle melting processes, it is useful to determine a strain-compensated partition coefficient D_0 [18]. Strain-compensation means that the redistributed element has the same charge and size as the regular element on the lattice site of the crystal [13]. Therefore, it is assumed that the radius of the element of interest r_i equals the lattice site radius r_0. This way the partition coefficient D_i can be calculated with the following equation:

$$D_i = D_0 \exp\left(\frac{-4\pi E_{M2} N_A (\frac{r_0}{2}(r_i - r_0)^2 + \frac{1}{3}(r_i - r_0)^3)}{RT}\right), \quad (1)$$

where E_{M2} is the bulk modulus of the M2 lattice site, N_A the Avogadro's number, R the gas constant and T the temperature. Here, the lattice site of interest is the crystallographic M2 site of clinopyroxene. Sodium is used as the strain-compensated partition coefficient D_0 because it is the 1+ charge element that has a radius r_i which is closest to the M2 lattice site radius r_0. Therefore, we assume $D_0 = D_{Na}$.

To calculate the strain-compensated partition coefficient D_0, we took a thermodynamic approach described by Blundy et al. (1995) [14]. For this, we used the melting curve of jadeite and linked it to the activity of jadeite's components in the melt. To calculate the partition coefficients of sodium between clinopyroxene and silicate melt, jadeite was the clinopyroxene of choice because of both, its high concentration in sodium and its ability to mix nearly ideally with diopside [19] and enstatite.

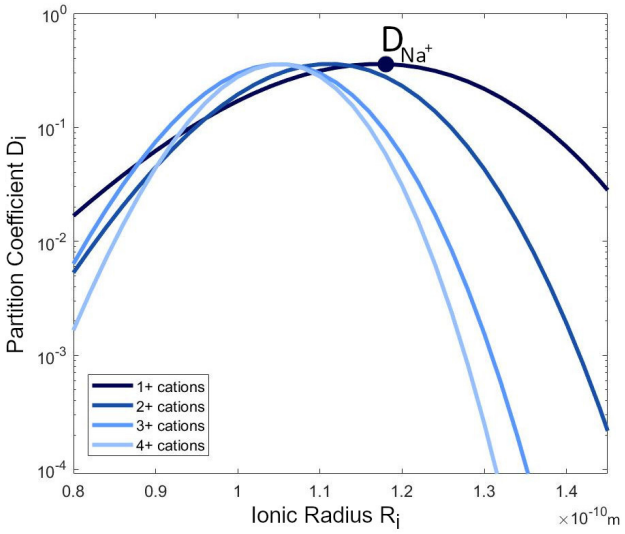

Figure 1. Partition coefficients of 1+ to 4+ charged cations in the clinopyroxene M2 lattice site. Modelled after Wood et al. (1997) [21]. Here, D_{Na} equals D_0.

Generally, partition coefficients are given as the weight fraction ratio

$$D_i = \frac{X_i^{crystal}}{X_i^{melt}}, \quad (2)$$

with X_i being the weight percentage of the given component. However, since we obtain partition coefficients with the help of thermodynamic properties, we calculate molar partition coefficients. Based on experiments on plagioclase/fluid partitioning [20], it is broadly assumed that also for other minerals molar partition coefficients nearly equal weight percentage coefficients [21]. Thus, we can make use of Flood's equation for exchange equilibria in molten salts [22]:

$$RT\ lnK_f = \sum N_i \Delta G^0, \quad (3)$$

where K_f is the molar equilibrium constant, N_i the concentration of the component and ΔG^0 the Gibbs' free energy of change. Because we use a thermodynamic approach for our calculations, N_i can be neglected and is set to one. The molar partitioning of jadeite D^{jd} can be expressed by using K_f in the expression

$$D_{jd} = \frac{1}{K_f} = \frac{n_{jd}^{cpx}}{n_{jd}^{melt}}, \quad (4)$$

where n_{jd}^{cpx} and n^{melt} are the mole of the solid clinopyroxene and molten components, respectively. Here, we assume an ideal case where the activity equals the mole fraction of the elements of interest. Thus, we assume $n_{jd}^{cpx} = X_{Na}^{cpx}$ and

$n_{jd}^{melt} = X_{Na}^{melt}$. Taking (4) and rearranging (3) leads to the following equation:

$$D_{Na}^{cpx/melt} = \exp\left(\frac{\Delta G_{f(P,T)}}{RT}\right). \quad (5)$$

Besides (5), one more equation is needed to determine D_{Na} thermodynamically. Equation (6) relates the entropy of the melting reaction to its heat capacity and melting point T_f of jadeite at the pressure P_f=0.0001 GPa. By including the enthalpy, we determine the Gibb's free energy change of reaction with the following equation:

$$\begin{aligned}\Delta G_{f(P,T)} =& \Delta H_{f(P_f,T_f)} + \int_{T_f}^{T} \Delta C_p dT \\ & - T\left(\Delta S_{f(P_f,T_f)} + \int_{T_f}^{T} \frac{\Delta C_p}{T} dT\right) \\ & + \int_{P_f}^{P} \Delta V_{f(T)} dP, \end{aligned} \quad (6)$$

where $\Delta H_{(f(P_f,T_f)}$ is the entropy, $\Delta S_{f(P_f,T_f)}$ the enthalpy and ΔC_p the difference between the local P,T values and P_f,T_f. $\Delta V_{f(T)}$ is the molar volume of fusion at pressure P_f extrapolated to the temperature of interest [14]. We calculate D_{Na} by inserting (6) into (5).

To be able to solve (6), we use the Maier-Kelly power function [23] to calculate the heat capacity C_p (as stated in Table I). With the given parameters we can solve the first two integrals in (6) analytically, by evaluating the heat capacity of the solid at temperature T and the melt heat capacity at T_f. To solve the third part of the integral in (6) we use a Riemann integral, where we approximate the intervals on subintervals defined over a pressure vector of n=1000 steps from P=0.0001 to 15 GPa and assume that the volumes of melt and solid are constant in each subinterval.

$$\begin{aligned}\int_{P_f}^{P} \Delta V_{f(T)} dP =& \sum_{i=1}^{n-1} \int_{P_i}^{P_{i+1}} \Delta V_{f(T),i} dP \\ \approx& \sum_{i=1}^{n-1} \Delta V_{f(T),i} \int_{P_i}^{P_{i+1}} dP \\ =& \sum_{i=1}^{n-1} \Delta V_{f(T),i} \left(P_{i+1} - P_i\right) \end{aligned} \quad (7)$$

where $\Delta V_{f(T),i}$ is the volume of fusion, i.e., the volume difference between melt and solids. The calculation of V_{solid} and V_{melt} is done separately using an isothermal Birch-Murnaghan equation of state:

$$P = 1.5K_T\left(x^{\frac{7}{3}} - x^{\frac{5}{3}}\right)\left(1 + 0.75(K' - 4)\left(x^{\frac{2}{3}} - 1\right)\right), \quad (8)$$

where $x = V^0/V$. K_T is the bulk modulus for pyroxene and K' its derivative. The volumes further depend on temperature via

$$V(T) = V \cdot \exp\left(\int_{T_0}^{T} \alpha^0(T) dT\right). \quad (9)$$

Here, we assume that the thermal expansion coefficient α^0 is constant for melts and solids (see Table I), hence

$$\begin{aligned}\Delta V_{f(T),i} =& \\ & V_{melt}(P_i) \cdot \exp\left(a_{melt}^0 (T - T_f)\right) \\ & - V_{solid}(P_i) \cdot \exp\left(a_{solid}^0 (T - T_0)\right). \end{aligned} \quad (10)$$

T_0 is set to 298 K. The partition coefficient D_{Na} is then derived for varied pressures and temperatures by inserting ΔG into (5).

TABLE I
THERMODYNAMIC INPUT DATA FOR LIQUID AND SOLID JADEITE AND COMPARISON OF MODEL PARAMETERS.

Parameters	Pyroxene	Melt	Units
V^0	60.4	79.9	kJ GPa^{-1}
α^0	2.81·10^{-5}	6.28·10^{-5}	K^{-1}
K_T	141.2	14.8	GPa
$\partial K/\partial T$	-0.025	-0.0015	GPa K^{-1}
K'	4.5	4.5	
$\Delta H_{f(0.1,T_f)}$	61.1±1.3		kJ mol^{-1}
$\Delta S_{f(0.1,T_f)}$	64.8±0.6		J mol^{-1}
T_f	943±22		K
C_p^a			
1	0.30113	0.28995[b]	kJ mol^{-1} K^{-1}
2	1.0143· 10^{-5}		kJ mol^{-1} K^{-1}
3	-2239.3		kJ mol^{-1} K^{-1}
4	-2.0551		kJ mol^{-1} K^{-1}

Parameters as in Blundy et al. (1995) [14] at 0.0001 GPa and 298 K (unless stated otherwise).
[a] $C_p = C_{p1} + C_{p2} \cdot T + C_{p3} \cdot T^{-2} + C_{p4} \cdot T^{-0.5}$ (T in kelvins).
[b] At temperatures >1200 K.

B. Scaling Law Development

The thermodynamic model indicates that partition coefficients are not only dependent on pressure, but temperature and therefore melt fraction as well. Thus, to develop a mantle melt fit function for the reference coefficient D_{Na}, we calculated partition coefficients between 0 and 15 GPa along the peridotite solidus temperature, peridotite liquidus temperature, and corresponding melt fraction F temperatures. The respective partition coefficients were determined with the thermodynamic approach described above. Melt fraction F is included because as is suggested by the batch melting equation [24], a rising melt fraction F leads to a decrease in the total amount of incompatible trace elements in the melt. Therefore, we arranged the melt fractions in $F = 0.2$ increments while neglecting the extraction of the melt, by using

$$F(P,T) = \frac{T - T(P)_{sol}}{T(P)_{liq} - T(P)_{sol}}. \quad (11)$$

The solidus T_{sol} and liquidus temperatures T_{liq} equations which we used [25] are third-order fits to experimental data

[26][27]:

$$T_{sol,ini} = 1409K + 134.2\frac{K}{GPa}\cdot P - 6.581\frac{K}{GPa^2}\cdot P^2 + 0.1054\frac{K}{GPa^3}\cdot P^3, \quad (12)$$

$$T_{liq,ini} = 2035K + 57.46\frac{K}{GPa}\cdot P - 3.487\frac{K}{GPa^2}\cdot P^2 + 0.0769\frac{K}{GPa^3}\cdot P^3. \quad (13)$$

For pressures from 0-15 GPa, the solidus temperatures range from 1409-2297 K, while the liquidus temperatures go from 2035-2372 K. The pressure step size for each temperature profile is 0.1 GPa, which corresponds to 151 D_{Na}-P-T data points for each melt temperature profile. With the least square function, these data points were fitted to a function with parameters a, b, c, d, e, and f (14) in Python 3. Because the function has the same form as the fit function of Blundy et al. (1995) [14], their fit parameters are compared in Table II.

$$\mathrm{D}_{Na}(\mathrm{T[K],P[GPa]}) = \exp\left(\frac{a + b\cdot P - c\cdot P^2}{T} - d + e\cdot P - f\cdot P^2\right). \quad (14)$$

By including the melt fraction P-T profiles, we make sure that the resulting model function will satisfy a broader range of P-T conditions and is not only valid for modelling partial melting in the mantle (where temperatures are close to the solidus), but also for crystallisation of melt (where temperatures are close to the liquidus). In contrast to our model, partition coefficients for crystallising liquid were often determined by taking only the liquidus temperatures into account [28][29][30].

Depending on the application (e.g magma ocean crystallisation or partial melt models), it may be advantageous to consider a narrower temperature/melt degree range, parametrised with a higher accuracy. For these parametrisations, we again used equations which calculate the respective temperatures from pressures in the range of 0-15 GPa. The stepsize of the pressure is again 0.1 GPa. For the parametrisation, we varied the temperature by $\pm$50 K along the melting curve to optimise the accuracy if there are smaller temperature diversions from the solidus (12) and liquidus (13) equations.

For both the thermodynamic model and the fit function development, replication data is accessible in the TRR170-DB [31].

C. Application to Other Trace Elements

To be able to model clinopyroxene/melt partition coefficients for anhydrous melts on the basis of D_{Na}, we mainly based our calculations on previous studies [21][32]. In these calculations, the melt composition is added to determine the bulk modulus E and lattice site radius r_0. The calculations are applicable to the M2 lattice site of clinopyroxene and ions with a 1+ charge. In the literature model [21], the method iterates the temperature over a fixed pressure until the clinopyroxene saturation in the melt is reached. For our model, however, we did not take the clinopyroxene saturation into account in favor of illustrating the partition coefficient without temperature adjustments for a fixed pressure.

As a first step in the model, the melt composition is given in weight% oxides (S_iO_2, T_iO_2, Al_2O_3, $Cr2O_3$, FeO, MnO, MgO, CaO, Na_2O, K_2O). As in [21], we consider iron only in the form of FeO. After adding temperature (in K) and pressure (in GPa) to the code, we converted the melt composition to moles and calculated the mol amounts of each cation to a total of 6 oxygen atoms in the melt. The resulting mol amounts are then used to determine the amount of the mineral components [21]:

$$Na = NaAlSi_2O_6\ (JD)$$

$$K = KAlSi_2O_6\ (KT)$$

$$Ti = CaTiAl_2O_6\ (CT)$$

$$(Al - 2Ti - Na - K) = CaAl_2SiO_6\ (CATS)$$

$$Ca - CaAl_2SiO_6 - CT = Ca(Mg, Fe, Mn)Si_2O_6\ (DI)$$

$$\tfrac{1}{3}[Mg + Fe + Mn - Ca(Mg, Fe, Mn)Si_2O_6] = (Mg, Fe, Mn)_3Si_{1.5}O_6\ (OL)$$

$$\tfrac{1}{3}[Si - 2K - 2Na - 2Ca(Mg, Fe, Mn)Si_2O_6 - CaAl_2SiO_6 - 1.5(Mg, Fe, Mn)_3Si_{1.5}O_6] = Si_3O_6\ (QZ).$$

Next, we calculated the model fraction of the jadeite component $NaAlSi_2O_6$ (X_{jd}^{cpx}) in the crystal with the following equation [14][21]:

$$\mathrm{X}_{jd}^{cpx}(T[K], P[GPa]) = JD\cdot\exp\left(\frac{10367 + 2100P - 165P^2}{T}\right) - 10.27 + 0.358P - 0.0184P^2. \quad (15)$$

To calculate the Ti content of the clinopyroxene M1 site X_{Ti}^{cpx}, we use the approximate relationship between CT in the liquid and X_{jd}^{cpx}:

$$X_{Ti}^{cpx} = CT\cdot(0.374 + 1.5X_{jd}^{cpx}). \quad (16)$$

We calculate the Cr content in the crystal M1 site X_{Cr}^{cpx} similarly:

$$X_{Cr}^{cpx} = 5Cr. \tag{17}$$

The activity of the $CaAl_2SoO_6$ component in clinopyroxne γ_{CaTs}^{cpx} is calculated from the product Ca for 6 oxygens in the liquid and Al per 6 oxygens:

$$\gamma_{CATS}^{cpx} = (CT + CATS + DI) \cdot (CATS + JD + KT) \cdot exp\left(\frac{76469 - 62.078T + 12430P - 870P^2}{8.314T}\right). \tag{18}$$

To be sure that pyroxene is not unrealistically aluminous, we apply an upper limit for the activity γ_{CaTs}^{cpx} of 0.4. The activity of the diopside component $CaMgSi_2O_6$ (DI) of the liquid γ_{Di}^{cpx} is calculated with the help of a parametrised parabolic pressure dependence of volume:

$$\gamma_{Di}^{cpx} = DI \cdot Mg\#_{melt} \cdot exp\left(\frac{132650 - 82.152T + 13860P - 1130P^2}{8.314T}\right). \tag{19}$$

With the activities calculated above, we calculate the Ca content of the M2 lattice site X_{Ca}^{M2}:

$$X_{Ca}^{M2} = \frac{\gamma_{CaTs}^{cpx} Mg\#_{melt} + \gamma_{Di}^{cpx}}{Mg\#_{melt}(1 - X_{Cr}^{cpx} - X_{Ti}^{cpx})}. \tag{20}$$

With the help of the activity of the CATS component γ_{CaTs}^{cpx} and the Ca content of the M2 lattice site X_{Ca}^{M2}, we are now able to calculate the lattice site radius r_0 [14]:

$$\mathrm{r_0} = 10^{-10}. \tag{21}$$

$$\left(\left(\frac{(0.974 + 0.067X_{Ca}^{M2})\ 0.051\gamma_{CaTs}^{cpx}}{X_{Ca}^{M2}}\right) + 0.12\right)[m].$$

In turn, the bulk modulus E is calculated as follows [14]:

$$E = (318.6 + 6.9P - 0.036T) \cdot \frac{1}{3}\ [GPa]. \tag{22}$$

For 1+ charge ions D_i^{1+}, (1) is slightly adjusted:

$$D^{1+} = D_{Na} \exp\left(\frac{-4\pi E_{M2} N_A (\frac{r_0}{2}(r_0^2 - r_i^2) + \frac{1}{3}(r_i^3 - r_0^3))}{RT}\right). \tag{23}$$

A detailed description of the adaptations to calculate partition coefficients for higher charges is also available in the literature [21][32]. For the model developed in this study, we used the programming language MATLAB.

III. Results

A. Thermodynamic Model Along Melting Temperature Profiles

In a pressure range between 0 and 15 GPa and a temperature range between 1400 and 2400 K, the thermodynamic model produces increasing partition coefficients from low P/high T (0 GPa/2400 K) to high P/low T (10-12 GPa/1400 K) conditions (Figure 2). The increase is in the order of four magnitudes and coincides with experimental observations [33][34]. At higher pressure above 12 GPa and low temperatures, the model starts to invert the trend and the partition coefficients decrease with increasing pressure. However, for our fit function development we have used the P-T space between the solidus and liquidus, which is not affected by this inversion. Along the melting temperature profiles, increasing pressure always leads to increasing partition coefficients, while increasing temperatures cause the partition coefficients to decrease (Figure 2).

In Table II, we compare the thermodynamic model results with experimental literature data. It is notable that most of the experimental data fit well to the model results. On average, the coefficients calculated by the thermodynamic model deviate from the experimental data by 26%. The best fitting value deviates only 2.9% from the experiments at 0.0001 GPa and 1526 K, while the worst fit deviates by 46.9% at 0.0001 GPa and 1524 K. The implications of this variance will be discussed in section IV.

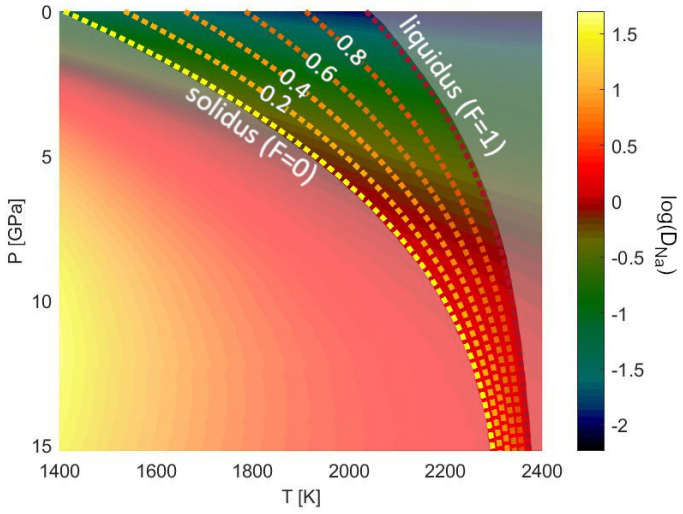

Figure 2. Clinopyroxene/melt partition coefficients for sodium in a P-T space, calculated thermodynamically with the methods of Blundy et al (1995) [14]. Solidus (12), liquidus (13) and intermediate melt fraction outlines are calculated from de Smet (1999) [25].

B. Parametrisation of Thermodynamic Model Results

As described in section II-B, we developed a scaled equation along the mantle peridotite solidus, liquidus, and corresponding melt fraction temperatures in between. For this, we used the least square function to fit the thermodynamic

TABLE II
COMPARISON OF EXPERIMENTAL DATA FOR CLINOPYROXENE/MELT PARTITION COEFFICIENTS WITH THE THERMODYNAMIC DATA

P [GPa]	T [K]	D_{Na} (experimental data)	Ref.	therm. model (this study)	Fit values by Blundy et al. (1995) [14]	Fit[a] (this study)
0.0001	1370	0.050(4)	[14]	0.0696	0.0670	0.0507[b]
0.0001	1449	0.042(4)	[14]	0.0496	0.0444	0.0465[b]
0.0001	1524	0.070(19)	[14]	0.0372	0.0312	0.0432[b]
0.0001	1526	0.040(4)	[14]	0.0369	0.0309	0.0431[b]
0.0001	1526	0.038(5)	[14]	0.0369	0.0309	0.0431[b]
0.0001	1598	0.046(5)	[14]	0.0288	0.0228	0.0404[b]
1	1663	0.075(7)	[14]	0.0891	0.0794	0.0991[b]
2	1773	0.113(8)	[14]	0.1708	0.1680	0.1827[b]
2	1843	0.144(13)	[14]	0.1363	0.1247	0.1587[b]
3	1938	0.237(30)	[14]	0.2241	0.2170	0.2465[b]
6	2038	0.52(12)	[14]	0.7789	0.6507*	0.7774
1.2	1588	0.225(5)	[35]	0.1497	0.1494	0.1366[b]
1.2	1458	0.221(5)	[35]	0.2671	0.3039	0.1807[b]
1.6	1643	0.283(4)	[35]	0.1866	0.1927	0.1750[b]

Parameter	Fit [14] 0-4 GPa	Fit[a] (this study) 4-12 GPa
a	10367	2183
b	2100	2517
c	165	-157
d	-10.27	-4.575
e	0.358	-0.5149
f	-0.0184	0.0475

D_{Na} is the experimentally determined weight partition coefficient.
[a] Parameters as in the scaling law fit for various melt fractions (24).
[b] Note that these are extrapolated values (beyond valid P-T range).
Parameters to be inserted into (14).

model results presented in Figure 2 to the following equation:

$$\mathrm{D}_{Na}(\mathrm{T[K]},\mathrm{P[GPa]}) = \exp\left(\frac{2183 + 2517P - 157P^2}{T} - 4.575 - 0.5149P + 0.0475P^2\right). \quad (24)$$

With the new resulting scaling law (24), it is now possible to calculate partition coefficients for sodium at varied temperature and pressure conditions.

Figure 3 illustrates how the rising D_{Na} values correlate with rising pressure along the solidus temperature. In contrast to the scaling law of Blundy et al. (1995) [14], our resulting scaling law produces steadily rising values up to 13.2 GPa at the respective peridotite solidus temperatures. After this point, the calculated values are starting to decrease. In contrast to our study, the model values of Blundy et al. (1995) [14] start to decline after approximately 5 GPa along the solidus temperature. However, Blundy et al. (1995) [14] themselves state that their scaling law is not to be used over a pressure of 4 GPa.

In Figure 4, the decrease of partition coefficients from the solidus towards the liquidus becomes visible. This indicates that not only pressure, but also temperature and therefore melt

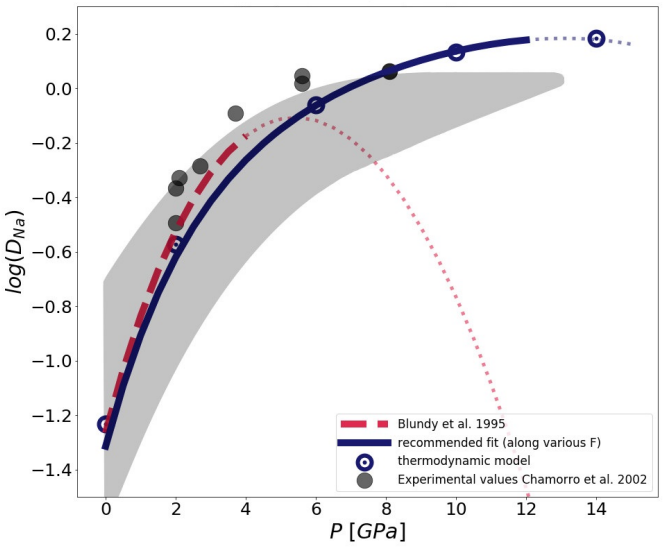

Figure 3. D_{Na} fits along the solidus from Blundy et al. (1995) [14] (red, dashed line) and this study (blue, solid line) compared to experimental data [34] (shaded grey area and grey dots) for comparison. Thin dotted lines are extrapolations of the fit functions beyond the range of validity.

fractions have an impact on the redistribution. It should be noted that at low pressures and high melt fractions, our fit seems to divert more from the thermodynamic model than the previous fit [14]. Consequences of this diversion on the

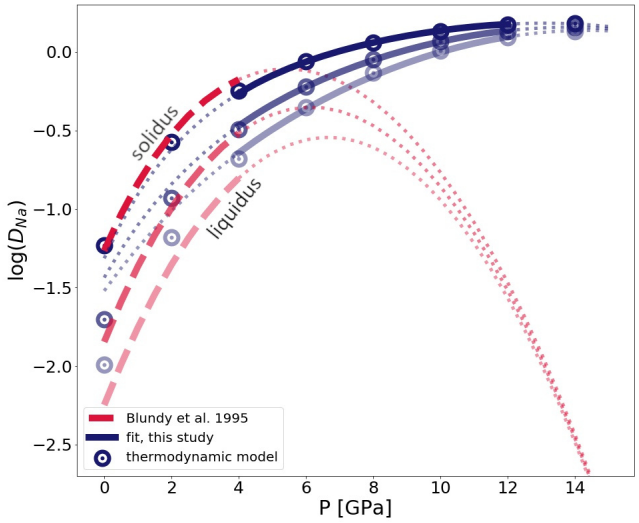

Figure 4. Partition coefficients depending on melt fractions. The line in between liquidus and solidus indicates a melt fraction F=0.5. Thin dotted lines are extrapolations of the fit functions beyond the range of validity.

applicability of our scaling law (24) are explored in section IV.

C. Application to Potassium

Potassium is a prominent radiogenic heat source in the Earth's mantle [16][17] and therefore an important trace element in mantle evolution models. Because potassium is, just like sodium, a 1+ charged element, D_{Na} can be used as an almost strain-free "reference" coefficient.

In Figure 5, we plotted the resulting potassium partition coefficients D_K over solidus P-T conditions with (1) the D_{Na} scaling law which can be found in the literature [14], (2) D_{Na} values modeled from the thermodynamic model, and (3) our D_{Na} scaling law fitted to higher pressures (24). The diagram shows that the D_K calculated with our scaling law (24) only diverts slightly from the D_K values which were calculated with the help of the thermodynamic model D_{Na} values: Below 4 GPa, the variation between the three models is negligible. The largest difference occurs at 12 GPa with a difference of 16.8%.

The scaling law from [14] also shows a good fit to the thermodynamic model in the range of its applicability (up to 4 GPa), but it diverts slightly more from the thermodynamic model than our own scaling law, which was fitted along these thermodynamic model values.

D. Solidus and Liquidus Scaling Laws

To avoid the wide spread between thermodynamic model and scaling law at low pressures (Figure 4), we created two more scaling laws for solidus and liquidus conditions, respectively. As described in section II-B, we added and substracted 50 K along (12) and (13) to ensure no large discrepancies with the thermodynamic model for small temperature perturbations. The results are presented in Figure 6 and the two new scaling laws along solidus and liquidus are, respectively:

$$\mathrm{D}_{Na}^{sol}(\mathrm{T[K],P[GPa]}) = \exp\left(\frac{2508 + 2333P - 138.5P^2}{T} - 4.514 - 0.4791P + 0.0415P^2\right), \quad (25)$$

$$\mathrm{D}_{Na}^{liq}(\mathrm{T[K],P[GPa]}) = \exp\left(\frac{-13728 + 4827P - 237P^2}{T} + 2.496 - 1.540P + 0.0829P^2\right). \quad (26)$$

As is shown in Figure 6, both scaling laws fit well to the thermodynamic model along their respective P-T conditions. However, the scaling laws seem to slightly overestimate the partition coefficients for D_{Na} at low pressures below approximately 4.5 GPa, while they underestimate the partition coefficients for higher pressures. This results in a small tilting of the scaling laws in respect to the thermodynamic model. As a consequence, the largest difference between solidus scaling law (25) and thermodynamic model is 33.5% at 15 GPa. For the liquidus scaling law (26), the largest difference is as well at 15 GPa with 29.8%.

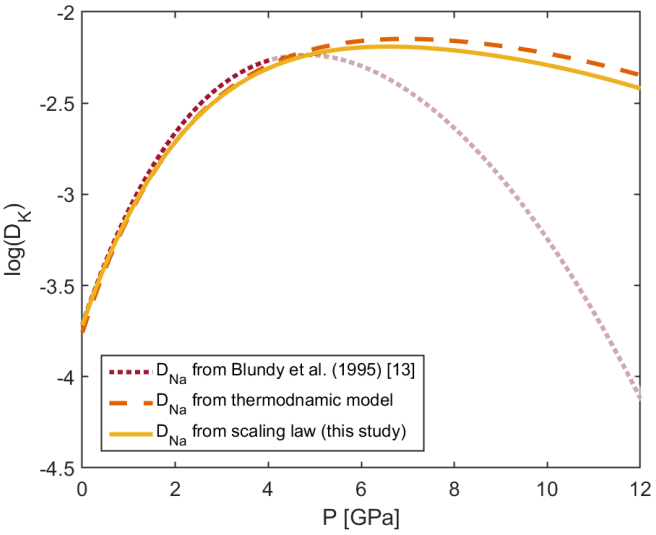

Figure 5. Potassium partition coefficients over solidus P-T conditions. Calculations are based on D_{Na} of either this study (24), thermodynamic model, and a model of Blundy et al. (1995) [14].

TABLE III
MELT STARTING COMPOSITIONS OF EXPERIMENTAL LITERATURE DATA.

	Hauri (1994) [36]	Hauri (1994) [36]	Hart and Dunn (1993) [37]	Klemme (2002) [38]	Salters and Stracke (2004) [39]	Salters and Stracke (2004) [39]
P [GPa]	2.5	1.7	3	3	3	2
T [K]	1703.15	1678.5	1653.15	1673.15	not specified[2]	not specified[2]
Si_O_2	46.7	46.7	47.67	56.7	46.18	57.53
Ti_O_2	0.5	0.5	2.67	6.3	1.45	0.59
Al_2O_3	18.0	18.0	16.06	19.3	25.29	16.28
$Cr2O_3$	0.0	0.0	0.0	0.0	0	0
FeO	8.03	8.03	10.88	0.0[1]	9.72	4.1
MnO	0.15	0.15	0.23	0.0[1]	0[1]	0[1]
MgO	9.52	9.52	5.91	4.2	15.49	5.27
CaO	12	12	9.5	6.8	7	6.99
Na_2O	2.05	2.05	3.92	3.3	2.71	6.87
K_2O	0.07	0.07	1.34	3.3	2.16	2.37
D_K	0.0067	0.0081	0.0072	0.007	0.0001	0.001

Melt composition of the experimental literature values stated in Figure 7 in wt%. For our example calculations, an alkaline basaltic melt composition was used [37].
[1]In order to calculate the partition coefficients with the method described in section II-C, values were adjusted to 0.0001.
[2] The authors did not specify the temperature. For Figure 7, the temperature was set to the corresponding solidus temperature.

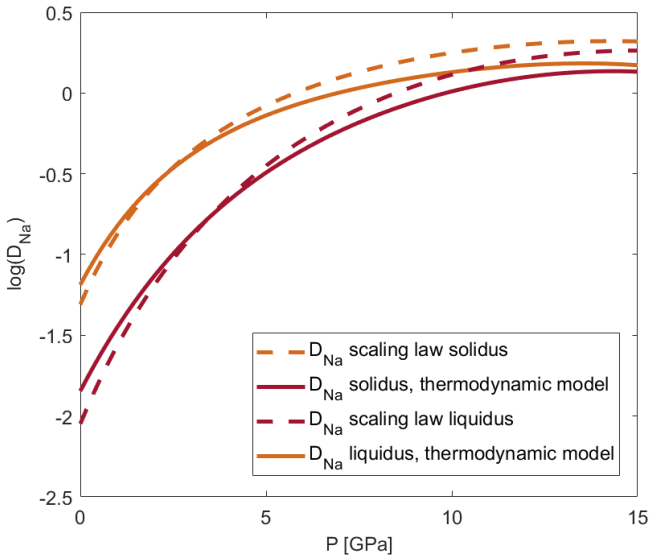

Figure 6. Scaling laws for parametrised solidus and liquidus [25].

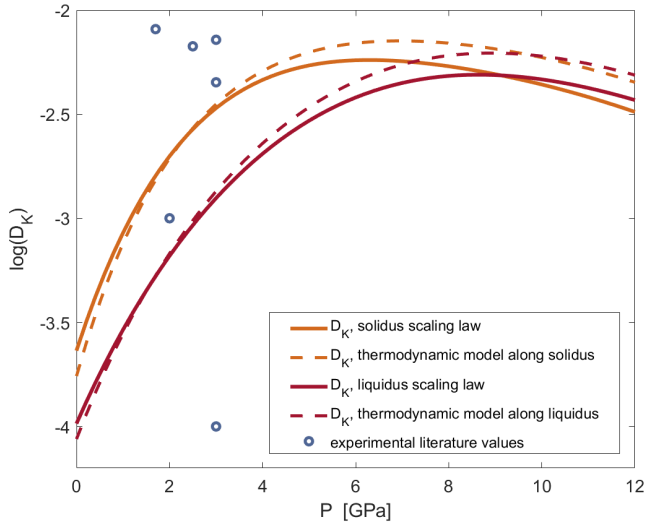

Figure 7. Scaling laws for parametrised solidus and liquidus [25]. Corresponding temperature and melt composition of the experimental literature values can be found in Table III.

In addition to the described D_K calculations in section III-C, we calculated D_K as well with the help of the solidus and liquidus scaling laws (Figure 7). As for D_{Na}, a variation can be observed between calculated D_{Na} from the thermodynamic model and from the scaling law for higher pressures. For the D_K calculations, we have used a literature alkali basaltic melt composition [37].

As a comparison, we plotted experimental literature values for the corresponding pressures against the calculated partition coefficients. The apparent wide spread of the data is discussed below in section IV-C.

The melt compositions of the experimental data as used in our calculations [36][37][38][39] can be found in Table III.

IV. DISCUSSION

A. Sodium Partitioning from low to higher Pressure

Partition coefficients are highly controlled by pressure, temperature, and composition. Since it is not possible for models to include all compositional interactions between a mineral and melt, comparing them to experimental data is sometimes difficult. This is especially true for higher pressures, where partition coefficient data is, to this date, often lacking. However, the existing experimental data for lower pressures already indicate if we can expect realistic results from our calculations. As is shown in Table II, our thermodynamic model results fit well to the experimental results [14][35]. Best matches were achieved for experimental

data at 0.0001 GPa/1526 K, 2 GPa/1843 K and 3 GPa/1938 K [14], where the model data deviates from the experimental values by only 2.9% and for the latter two by 5.4%, respectively. Interestingly, with 46.9%, the second largest diversion from the experimental data is at 0.0001 GPa/1524 K, which is at the same pressure and only 2 K below a very well fitting value (Table II). However, the experimentally derived partition coefficients vary more than what could be solely explained by changing P-T conditions. Deviating experimental and thermodynamic model results can happen because of several effects. For example, analytical error margins have to be considered. Furthermore, the composition of melt as well as solid clinopyroxene can be much more diverse in experiments than it is for thermodynamic model calculations, which does not take these changes into account.

It should be noted that the fit parameters in (14) differ from the parametrisation in Blundy et al. (1995) [14], which is due to the larger parameter space applied in our model. For a comparison of the two scaling laws for various melt fractions, we refer to Figure 3 and Figure 4. A direct comparison of the resulting parameters for our scaling law (24) and the previous study [14] is given in Table II.

Figure 3 illustrates that the partition coefficients calculated with our scaling law (24) over solidus temperatures is close to the experimental sodium partitioning data. This data is indicated by a shaded grey area and, for D_{Na} in the $Ab_{80}Di_{20}$ system, by darker grey dots [34]. A direct comparison with appropriate temperatures in the range of the experimental data [34] shows that here, the thermodynamic model is within an error of on average 32%.

As is shown in Figure 3 and Figure 4, our and the previous fit [14] do not completely agree with each other. Blundy et al. (1995) [14] parametrised their thermodynamically calculated results over a peridotite solidus of McKenzie and Bickle (1988) [40], while we took the peridotite solidus equation of de Smet (1999) [25]. This could have produced a small shift in the D_{Na}-P-T field and, therefore, in the resulting fit function. Also, a different parametrisation method could have been used by the previous study [14], which might have produced slightly different fits. Finally, the previous study [14] concentrated more on low pressure partitioning, whereas we have tried to parametrise the function up to the 410 km discontinuity. The inclusion of higher pressures could also be the reason why at pressures below 4 GPa (especially at higher melt fractions) our scaling law (24) fits less well to the thermodynamic model values than the older model [14].

Between 4 and 12 GPa, our scaling law (24) fits well to the thermodynamic data over all melt fraction values from solidus to liquidus. However, at high melt fractions below 4 GPa, larger diversions from the original fit function [14] appear (Figure 4). The reason for this lies in the nature of the least square parametrisation used in Python 3, which allows the scaling law to divert from the thermodynamic model at low pressures for the expense of being applicable to higher pressures and to a wide range of melt fractions. If we would only parametrise the model over the solidus, the shift would disappear at the expense of the model being applicable to any other P-T conditions. Thus, the included P-T conditions for the varying melt fractions ensure that the model is useful over a wide range of pressures and temperatures, but limits the applicability of the scaling law for higher melt fractions to a range between 4 and 12 GPa.

In the upper mantle, buoyant melt can occur up to the depth where it becomes gravitationally stable and a density inversion of melt and solid surrounding material takes place (the so-called density crossover). In other words, melts formed at higher pressures may not be able to rise to the surface [41][42]. However, this is only true for upper mantle melts and melts rising upwards in lower regions of the Earth can not be ruled out [43]. Inside Earth, the density crossover exists at approximately 11-12 GPa at 2000°C [44], and in Mars between 7 GPa [44] and 7.5 GPa [45]. To include pressure and temperature dependent partition coefficients into a mantle evolution model, it would often suffice to be able to calculate them up to the density crossover. Overlapping with the density crossover, in the Earth's 410 km mantle discontinuity (i.e., pressures of approximately 12-15 GPa), phase changes occur [46] and pyroxene slowly starts to dissolve into a pyrope-rich garnet to form majorite [47]. This and the density crossover indicate that a parametrise up to approximately 12-15 GPa is sufficient.

As the experimental data [33][34] suggests, the partition coefficients of sodium in clinopyroxene increase with temperature and pressure before they remain constant. At solidus P-T conditions, our fit function curve slowly starts to flatten and starts to fall at approximately 13 GPa (Figure 3). This coincides with the thermodynamic model, where (along the solidus) the partition coefficients start to decrease at 12.5 GPa. Combining these findings with the occurence of a density crossover and transition zone at approximately 12 GPa, we suggest to not use our scaling law (24) above this pressure.

As is discussed above, the scaling law (24) works well for melting P-T conditions between the peridotite solidus and liquidus between 4 and 12 GPa. Thus, it can be considered as a useful expansion of the previous scaling law for D_{Na} [14]. Because of the broad P-T range, the model should not only be useful for mantle melting, but also for models which crystallise melt, as is the case in a magma ocean. However, as recent studies have suggested, the solidus and liquidus temperature may change heavily depending on if material is melting or crystallising [48]. If this is the case, our model could lie outside of the P-T range between solidus and liquidus for crystallising liquids and would have to be extrapolated. Therefore, one has to be careful with the usage of the fits.

B. Solidus and Liquidus Scaling Law

To avoid the usage of two scaling laws to cover the pressure range of 0-12 GPa, we developed separate scaling laws which are only useful along the solidus and liquidus P-T conditions.

It is shown in Figure 6 that, in contrast to the scaling law for various melt fractions (24), especially the liquidus scaling law (26) fits much better to the thermodynamic model than the more general approach (24) and works just as well as the scaling law of the previous study for low pressures [14]. As a consequence, along the liquidus it is possible to use the respective scaling law (26) over the pressure range 0-12 GPa.

Along the solidus, the general scaling law over various melt fractions (24) fits well to the thermodynamic model (Figure 3). In fact, it seems to fit slightly better to the thermodynamic model than the solidus scaling law (25). As a conclusion, it might not have a big impact if either the solidus scaling law or the more general scaling law are used from 0-12 GPa along solidus temperatures.

C. Potassium Partitioning

To calculate clinopyroxene/melt partition coefficients for potassium, we have used D_{Na} as a nearly strain-free "reference" coefficient as described in section II. In Figure 5, the general D_{Na} scaling law (24) leads to a very good fit of D_K when comparing the thermodynamic D_{Na} approach with the scaling law. In contrast to that, Figure 7 shows D_K values calculated with the solidus and liquidus scaling laws and compares them to experimental data. The experimental data exhibits a very wide spread for close pressure ranges. This spread can occur because (1) the experimental values were measured for different temperatures, (2) the composition of the melt differs, (3) components in the experimental starting composition were neglected in our calculations but lead to additional chemical reactions and influence the partition coefficients.

D. Application to other Terrestrial Planets

Just as the thermodynamic model, phase transitions and density crossover behaviour all depend on pressure. Thus, even for planets with a radius or mass different from Earth, the fit should be applicable if the mantle composition is comparable to Earth. Additionally, the mineralogy of the terrestrial planet has to be taken into account. If there is no or if there are only very minor portions of clinopyroxene in the planets upper mantle, our partition coefficient calculations for clinopyroxene cannot be used.

V. Conclusion and Future Work

With the new high-pressure scaling laws (24)-(26), it is now possible to include partition coefficient models depending on pressure and temperature into mantle convection models for the entire pressure range over which upper mantle melts are buoyant. The newly developed fit functions can be used to calculate clinopyroxene/melt redistribution behaviour of sodium starting from 0 or 4 GPa up to the mantle transition zone of the Earth. This is in contrast to the scaling law by Blundy et al. (1995) [14], which can be applied only from 0 to 4 GPa. We apply our new scaling laws as basis for calculating the partition coefficients for 1+ charge element D_K with (23). Possible approaches to model clinopyroxene/melt partition coefficients for the charges 2+ to 4+ are described in Wood and Blundy (2014) [32] and are based on adjusted calculations for the mineral's lattice site radius r_0 and the bulk modulus E.

Compared to the existing experimental data, our scaling law (24) allows for a good approximation of clinopyroxene partition coefficients of trace elements between solid and melt. This enables us to do self-consistent calculations of local partition coefficients for variable pressures and temperatures. Because we parametrise our scaling law (24) over a wide range of P-T conditions and melt fractions between the peridotite solidus and liquidus, our model can be applied for any $D_{Na}^{cpx/melt}$ calculation between 1850-2360 K and 4-12 GPa. However, if only the solidus or liquidus conditions are needed, the respective scaling laws (25) and (26) might be more useful, as they can be used over the whole range of 0-12 GPa.
The new, higher-pressure-tolerant scaling laws enable us to model the redistribution of trace elements in terrestrial planets in much more detail. Our partition coefficient calculations for clinopyroxene should be applicable as long as clinopyroxene is present in the planet's upper mantle in sufficient abundance.

Future works could not only include the application of our scaling laws in numerical simulations, but also further investigations on partitioning behaviour in mantle material as well. For instance, adding an orthopyroxene/melt trace element partitioning model to a mantle evolution model would provide an even more detailed tool to study on the trace element redistribution from mantle to crust if used alongside the clinopyroxene/melt partitioning model. Furthermore, it is known that water lowers partition coefficients significantly [49]. Consequently, our models would greatly benefit from additional adaptations for water-saturated melts.

For the thermodynamic model, fit function development, and the partitioning of the 1+ charge elements in clinopyroxene/melt, the source code is available in the TRR170-DB [31].

Acknowledgment

We would like to thank Jon Blundy and Timm John for fruitful discussions on partition coefficient modelling. This study was funded by the Deutsche Forschungsgemeinschaft (DFG, German Research Foundation) – Project-ID 263649064 – TRR 170. This is TRR 170 Publication No. 147.

References

[1] J. M. Schmidt and L. Noack "Parametrising a Model of Clinopyroxene/Melt Partition Coefficients for Sodium to Higher Upper Mantle Pressures", GEOProcessing conference 2021, July 2021.

[2] H. Neumann, J. Mead, and C. Vitaliano "Trace element variation during fractional crystallization as calculated from the distribution law," Geochimica et Cosmochimica Acta, vol. 6 (2-3), pp. 90-99, February 1954.

[3] P. W. Gast "Trace element fractionation and the origin of tholeiitic and alka-line magma types," Geochimica

et Cosmochimica Acta, vol. 32 (10), pp. 1057-1086, October 1968.

[4] B. B. Jensen "Patterns of trace element partitioning," Geochimica et Cosmochimica Acta, vol. 37 (10), pp. 2227-2242, October 1973.

[5] K. T. Johnson, H. J. Dick, and N. Shimizu "Melting in the oceanic upper mantle: an ion microprobe study of diopsides in abyssal peridotites," Journal of Geophysical Research: Solid Earth, 95 (B3), 2661-2678, March 1990.

[6] T. Skulski, W. Minarik, and E. B. Watson, E. B. "High-pressure experimental trace-element partitioning between clinopyroxene and basaltic melts," Chemical Geology, vol. 117 (1-4), pp. 127-147, November 1994.

[7] U. Walzer, and R. Hendel "Mantle convection and evolution with growing continents" Journal of Geophysical Research: Solid Earth, vol. 113 (B9), September 2008.

[8] A. Morschhauser, M. Grott, and D. Breuer "Crustal recycling, mantle dehydration, and the thermal evolution of Mars," Icarus, vol. 212 (2), pp. 541-558, April 2011.

[9] T. Ruedas, P. J. Tackley, and S. C. Solomon "Thermal and compositional evolution of the martian mantle: Effects of phase transitions and melting," Physics of the Earth and Planetary Interiors, vol. 216 , pp. 32-58, March 2013.

[10] A.-C. Plesa, and D. Breuer "Partial melting in one-plate planets: Implications for thermo-chemical and atmospheric evolution," Planetary and Space Science, vol-405 98 , pp. 50-65, August 2014.

[11] R. E. Jones, P. E. van Keken, E. H. Hauri, J. M. Tucker, J. Vervoort, and C. J. Ballentine "Origins of the terrestrial Hf-Nd mantle array: evidence from a combined geodynamical-geochemical approach," Earth and Planetary Science Letters, vol. 518 , pp. 26-39, July 2019.

[12] V. M. Goldschmidt "The principles of distribution of chemical elements in minerals and rocks," Journal of the Chemical Society (Resumed), pp. 655-673, March 1937.

[13] J. Brice "Some thermodynamic aspects of the growth of strained crystals," Journal of Crystal Growth, vol. 28 (2), pp. 249-253, March 1975.

[14] J. Blundy, T. Falloon, B. Wood, and J. Dalton "Sodium partitioning between clinopyroxene and silicate melts," Journal of Geophysical Research: Solid Earth, vol. 340 100 (B8), pp. 15501-15515, August 1995.

[15] J. M. Schmidt and L. Noack "Modelling clinopyroxene/melt partition coefficients for higher upper mantle pressures," EGU General Assembly 2021, online, EGU21-12478, https://doi.org/10.5194/egusphere-egu21-12478, April 2021.

[16] R. Arevalo Jr, W. F. McDonough, and M. Luong "The K/U ratio of the silicate Earth: Insights into mantle composition, structure and thermal evolution," Earth and Planetary Science Letters, vol. 278(3-4), pp. 361-369, February 2009.

[17] A. Gando, D. A. Dwyer, R. D. McKeown, and C. Zhang "Partial radiogenic heat model for Earth revealed by geoneutrino measurements," Nature geoscience, vol. 4(9), pp. 647-651, July 2011.

[18] P. McDade, J. D. Blundy, and B. J. Wood "Trace element partitioning on the Tinaquillo Lherzolite solidus at 1.5 GPa," Physics of the Earth and Planetary Interiors, vol. 139 (1-2), pp. 129-147, September 2003.

[19] B. J. Wood, and J. Nicholls "The thermodynamic properties of reciprocal solid solutions," Contributions to Mineralogy and Petrology, vol. 66 (4), pp. 389-400, June 1978.

[20] J. Blundy, and B. Wood "Crystal-chemical controls on the partitioning of Sr and Ba between plagioclase feldspar, silicate melts, and hydrothermal solutions," Geochimica et Cosmochimica Acta, vol. 55 (1), pp. 193-209, January 1991.

[21] B. J. Wood, and J. D. Blundy "A predictive model for rare earth element partitioning between clinopyroxene and anhydrous silicate melt," Contributions to Mineralogy and Petrology, vol. 129 (2-3), pp. 166-181, October 1997.

[22] K. Grjotheim, C. Krohn, and J. Toguri "Thermodynamic evaluation of activities in molten mixtures of reciprocal salt systems," Transactions of the Faraday Society, vol. 57 , pp. 1949-1957, March 1961.

[23] C. G. Maier, and K. Kelley "An equation for the representation of high-temperature heat content data," Journal of the American chemical society, vol. 54 (8), pp. 3243-3246, August 1932.

[24] J. Hertogen, and R. Gijbels "Calculation of trace element fractionation during partial melting," Geochimica et Cosmochimica Acta, vol. 40 (3), pp. 313-322, March 1976.

[25] J. De Smet, A. Van Den Berg, and N. Vlaar, N. "The evolution of continental roots in numerical thermo-chemical mantle convection models including differentiation by partial melting," In: Developments in geotectonics. Elsevier, vol. 24, pp. 153-170, 1999.

[26] T. Gasparik "Phase relations in the transition zone," Journal of Geophysical Research: Solid Earth, vol. 95 (B10), pp. 15751-15769, September 1990.

[27] E. Takahashi "Speculations on the Archean mantle: missing link between komatiite and depleted garnet peridotite," Journal of Geophysical Research: Solid Earth, vol. 95 (B10), pp. 15941-15954, September 1990.

[28] D. C. Presnall, Y.-H. Weng, C. S. Milholland, and M. J. Walter "Liquidus phase relations in the system MgO-MgSiO3 at pressures up to 25 GPa - constraints on crystallization of a molten Hadean mantle," Physics of the Earth and Planetary Interiors, vol. 107 (1-3), pp. 83-95, April 1998.

[29] M. Walter, E. Nakamura, R. Tronnes, R., and D. Frost, D. "Experimental constraints on crystallization differentiation in a deep magma ocean," Geochimica et Cosmochimica Acta, vol. 68 (20), pp. 4267-4284, October 2004.

[30] D. M. Shaw "Trace element fractionation during anatexis," Geochimica et Cosmochimica Acta, vol. 34 (2),

pp. 237-243, February 1970.

[31] J. M. Schmidt, and L. Noack "Replication Data for: Clinopyroxene/Melt Partitioning: Models for Higher Upper Mantle Pressures Applied to Sodium and Potassium," TRR170-DB, (V01), 2021, doi.org/10.35003/GIAZCQ.

[32] B. J. Wood, and J. D. Blundy, J. D. (2014) "Trace element partitioning: The influences of ionic radius, cation charge, pressure, and temperature," In H. D. Holland and K. K. Turekian (Eds.), Treatise on geochemistry (second edition) (Second Edition ed., p. 421 - 448). Oxford: Elsevier, 2014.

[33] W. Wang, and E. Takahashi "Subsolidus and melting experiments of a K-rich basaltic composition to 27 GPa: Implication for the behavior of potassium in the mantle," American Mineralogist , vol. 84 (3), pp. 357-361, November 1999.

[34] E. Chamorro, R. Brooker, J. A. Wartho, B. Wood, S. Kelley, and J. Blundy "Ar and K partitioning between clinopyroxene and silicate melt to 8 GPa," Geochimica et Cosmochimica Acta, vol. 66 (3), pp. 507-519, February 2002.

[35] G. A. Gaetani, A. J. Kent, T. L. Grove, I. D. Hutcheon, and E. M. Stolper "Mineral/melt partitioning of trace elements during hydrous peridotite partial melting," Contributions to Mineralogy and Petrology, vol. 145 (4), pp. 391-405, May 2003.

[36] E. H.Hauri, T. P. Wagner, and T. L. Grove "Experimental and natural partitioning of Th, U, Pb and other trace elements between garnet, clinopyroxene and basaltic melts," Chemical Geology, vol. 117(1-4), pp. 149-166, 1994.

[37] S. R. Hart and T. Dunn "Experimental cpx/melt partitioning of 24 trace elements," Contributions to Mineralogy and Petrology, vol. 113(1), pp. 1-8, 1993.

[38] S. Klemme, J. D. Blundy, B. J. Wood "Experimental constraints on major and trace element partitioning during partial melting of eclogite," Geochimica et Cosmochimica Acta, vol 66(17), pp. 3109-3123, 2002.

[39] V. J. Salters, A. Stracke "Composition of the depleted mantle," Geochemistry, Geophysics, Geosystems, vol. 5(5), 2004

[40] D. Mckenzie, and M. Bickle "The volume and composition of melt generated by extension of the lithosphere," Journal of petrology, vol. 29 (3), pp. 625-679, June 1988.

[41] E. Stolper, D. Walker, B. H. Hager, and J. F. Hays "Melt segregation from partially molten source regions: the importance of melt density and source region size," Journal of Geophysical Research: Solid Earth, vol. 86 (B7), pp. 6261-6271, July 1981.

[42] Z. Jing, and S.-i. Karato "The density of volatile bearing melts in the Earth's deep mantle: The role of chemical composition," Chemical Geology, vol. 262 (1-2), pp. 100-107, May 2009.

[43] M. J. Beuchert and H. Schmeling "A melting model for the lowermost mantle using Clapeyron slopes derived from experimental data: Consequences for the thickness of ultralow velocity zones (ULVZs)," Geochemistry, Geophysics, Geosystems, vol. 14 (1), pp. 197-208, January 2013.

[44] E. Ohtani, Y. Nagata, A. Suzuki, and T. Kato "Melting relations of peridotite and the density crossover in planetary mantles," Chemical Geology, vol. 402 120 (3-4), pp. 207-221, March 1995.

[45] L. T. Elkins-Tanton, E. Parmentier, and P. Hess "Magma ocean fractional crystallization and cumulate overturn in terrestrial planets: Implications for Mars," Meteoritics & Planetary Science, vol. 38 (12), pp. 1753-1771, January 2003.

[46] A. E. Ringwood, A. E. "Phase transformations and their bearing on the constitution and dynamics of the mantle," Geochimica et Cosmochimica Acta, vol. 55 (8), pp. 2083-2110, August 1991.

[47] M. Akaogi "Phase transitions of minerals in the transition zone and upper part of the lower mantle," Special Papers-Geological Society Of America, vol. 421 , p. 1, 2007.

[48] C.-E. Boukare, Y. Ricard, and G. Fiquet "Thermodynamics of the MgO-FeO-SiO2 system up to 140 GPa: Application to the crystallization of Earth's magma ocean," Journal of Geophysical Research: Solid Earth, vol. 120 (9), pp. 6085-6101, August 2015.

[49] J. Blundy and B. Wood "Partitioning of trace elements between crystals and melts," Earth and Planetary Science Letters, vol. 210(3-4), pp. 383-397, January 2003.